Provided for non-commercial research and education use.
Not for reproduction, distribution or commercial use.

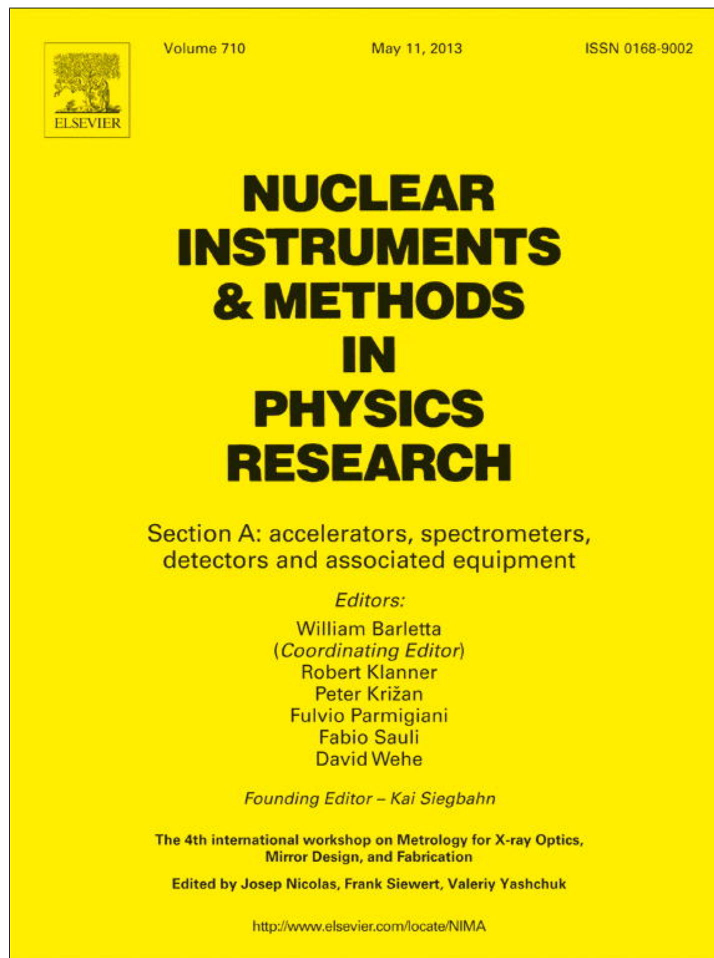

This article appeared in a journal published by Elsevier. The attached copy is furnished to the author for internal non-commercial research and education use, including for instruction at the authors institution and sharing with colleagues.

Other uses, including reproduction and distribution, or selling or licensing copies, or posting to personal, institutional or third party websites are prohibited.

In most cases authors are permitted to post their version of the article (e.g. in Word or Tex form) to their personal website or institutional repository. Authors requiring further information regarding Elsevier's archiving and manuscript policies are encouraged to visit:

http://www.elsevier.com/authorsrights

Author's personal copy

Nuclear Instruments and Methods in Physics Research A 710 (2013) 120–124

Contents lists available at SciVerse ScienceDirect

Nuclear Instruments and Methods in Physics Research A

journal homepage: www.elsevier.com/locate/nima

Polarization properties of Mo/Si multilayers in the EUV range

S. Uschakow [a], A. Gaupp [b], M. Gerhard [c], M. MacDonald [d], F. Schäfers [a,*]

[a] Institute for Nanometre Optics and Technology, HZB-BESSY-II, Albert-Einstein-Strasse 15, D-12489 Berlin, Germany
[b] Department Undulators, HZB-BESSY-II, Albert-Einstein-Strasse 15, D-12489 Berlin, Germany
[c] Zeiss SMT GmbH, 73447 Oberkochen, Germany
[d] Canadian Light Source Inc., Saskatoon, Canada

ARTICLE INFO

Available online 19 November 2012

Keywords:
EUV-radiation
Polarization properties
Mo/Si multilayer
Phase retardance
Reflectance
Block bootstrap

ABSTRACT

We investigate polarization properties of two novel reflective Mo/Si multilayers (ML) in the EUV range using polarized synchrotron radiation at the BESSY-II storage ring facility. One of the Mo/Si ML is used as a retarder, the other one as an analyzer within the experimental setup of the BESSY soft-x-ray polarimeter. The analyzer multilayer is characterized by performing reflectivity measurements with s- and p-polarized light as a function of the incidence angle for different wavelengths. The characterization of the retarder multilayer consists of reflectivity measurements with s- and p-polarized light as a function of the wavelength for three different angles near normal incidence. In addition the phase retardance on reflection was determined for one angle of incidence as function of wavelength. Uncertainties of the phase retardance are estimated via the block bootstrap method. As an additional by-product of the ML characterization the Stokes parameters of the beamline could be determined. With the 8-axis BESSY polarimeter we have measured the complex reflection coefficients for the first time and established this ellipsometry technique as an additional probe to characterize multilayer optical elements.

© 2012 Elsevier B.V. All rights reserved.

1. Introduction

High-reflectivity Mo/Si ML coatings operating in near-normal incidence geometry are required for the next generation of EUV-lithography at 13.5 nm [1]. Up to now such optical coatings are routinely characterized by reflectivity measurements. Optical imaging in EUV lithography requires both uniform reflection over different incidence angles and control over polarization effects, i.e. the phase retardance of the incident light upon reflection by the mirror. At present the latter information is obtained from coating models. In future EUV-systems with a higher angular load on the mirrors due to the increased numerical aperture the polarization dependent phase behavior will become more important. The phase behavior might have a detrimental effect on the contrast of the illuminated structure. A verification of the ML-model becomes necessary for the next generation lithography. Therefore at-wavelength metrology and polarimetry is a very desirable tool for the characterization of high-quality ML EUVL optical systems [2]. With the 8-axis BESSY polarimeter [3] which is routinely used to characterize ML optical elements for polarimetry purposes in the water window range [4] and at XUV energies [5,6] we have measured the reflection coefficients R_s and R_p and the relative phase retardance of the s and p components of the light reflected from the Mo/Si ML [7]. To have a meaningful and quantitative comparison between the simulation of the coating model and the measured data the uncertainties of the measured phase retardance are required. For this reason the block bootstrap method is introduced.

2. Experiment

The reflectivity and ellipsometry measurements were performed with the BESSY soft-x-ray polarimeter [3] that was upgraded to allow polarimetry measurements with both optical elements in reflection mode [8]. The principle of the polarimeter is based on the independent rotation of two optical elements around the light axis by the angles β and γ while the intensity is recorded by a polarization insensitive detector (GaAs Schottky photo diode). The first optical element is the retarder, which introduces a phase retardance Δ between s- and p-waves upon reflection. It is realized by a Mo/Si ML with a grazing angle of incidence θ_A. The second optical element is the analyzer with an angle of incidence θ_γ. For the present work this is also a Mo/Si ML with the Bragg angle set to near the Brewster angle at

* Corresponding author.
E-mail addresses: sergej.uschakow@helmholtz-berlin.de (S. Uschakow), andreas.gaupp@helmholtz-berlin.de (A. Gaupp), mike.macdonald@lightsource.ca (M. MacDonald), franz.schaefers@helmholtz-berlin.de (F. Schäfers).

0168-9002/$ - see front matter © 2012 Elsevier B.V. All rights reserved.
http://dx.doi.org/10.1016/j.nima.2012.10.133

Author's personal copy

approximately 45°. Radiation that passes the polarimeter and hits the detector is described by the Stokes vector QUOTE D. Assuming that the detector is polarization insensitive the measured signal S_{D0} is given by the polarimetry equation [3,9,10]:

$$S_{Do}(S_o,S_1,S_2,S_3,\psi_1,\psi_2,\Delta,\beta,\gamma)=\left(\frac{1}{2}\left(|r_s^{(1)}|^2+|r_p^{(1)}|^2\right)\right)$$
$$\left(\frac{1}{2}\left(|r_s^{(2)}|^2+|r_p^{(2)}|^2\right)\right)S_o\{(1+\cos 2\psi_1\cos 2\psi_2\cos(2\beta-2\gamma))\}$$
$$+\left(\frac{S_1}{S_0}\right)\left[\cos 2\psi_1\cos 2\beta+\frac{1}{2}(1+\sin 2\psi_1\cos\Delta)\cos 2\psi_2\cos 2\gamma\right.$$
$$\left.+\frac{1}{2}(1-\sin 2\psi_1\cos\Delta)\cos 2\psi_2\cos(4\beta-2\gamma)\right]$$
$$+\left(\frac{S_2}{S_0}\right)\left[\cos 2\psi_1\sin 2\beta+\frac{1}{2}(1+\sin 2\psi_1\cos\Delta)\cos 2\psi_2\sin 2\gamma\right.$$
$$\left.+\frac{1}{2}(1-\sin 2\psi_1\cos\Delta)\cos 2\psi_2\sin(4\beta-2\gamma)\right]$$
$$+\left(\frac{S_3}{S_0}\right)[\sin 2\psi_1\cos 2\psi_2\sin\Delta\sin(2\beta-2\gamma)]\} \quad (1)$$

The polarimetry equation includes seven unknown variables, namely the four Stokes parameters (S_0, S_1, S_2, S_3) describing the source, the polarization properties of the retarder (Δ) and $\psi_1=\arctan(|r_p^{(1)}|/|r_s^{(1)}|)$ and of the analyzer $\psi_2=\arctan(|r_p^{(2)}|/|r_s^{(2)}|)$. In the next chapter these seven variables are collectively noted as a, $r_s^{(1,2)}$ and $r_p^{(1,2)}$ are the complex reflection coefficients in s- and p-geometry of the first and second ML respectively.

The measurements are performed at the plane grating monochromator beamline PGM-1 [11] connected to the APPLE-II type undulator [12] UE56/2 at the BESSY-II storage ring facility. The spectral resolution is 0.1 eV using a grating with 400 l/mm, a front-end aperture of 2×2 mm^2 at 13 m from the source and a fix-focus constant of $c_{ff}=1.4$. By choosing this fix-focus constant value the monochromator operates in high order suppression mode. A beryllium filter was set into the beam path to further reduce the higher order contribution of the radiation. All measured signals are normalized to the ring current.

3. Block bootstrap

To have a quantitative comparison between the experiment and the ML coating model the quality of the estimated parameters has to be considered. In general, given a set of measured data and a known model function $f(x,a)$, the unknown parameter vector $a=\{(a_j,j=1,\ldots m)\}$ can be estimated using a fitting technique such as nonlinear least χ^2-fit. Each individual measurement y_i has an uncertainty σ_{yi}, that is included in the χ^2 definition. Minimizing χ^2 leads to an optimal parameter vector $\hat{a}$. To get the uncertainties σ_{aj} of $\hat{a}_j$ one calculates the second derivative of χ^2 at $a=\hat{a}$

$$\left(\frac{\partial^2\chi^2(\hat{a})}{\partial^2\hat{a}_j}\right)=\frac{2}{\sigma^2{}_{a_j}}=2C_{jj}^{-1} \quad (2)$$

The standard error σ_{aj} can also be calculated by determining the inverse of the covariance matrix C.

The measurement uncertainties σ_{yj} are required to estimate σ_{aj}. In many practical applications the measurement uncertainties are poorly known and only doubtful approximations can be made to σ_{yj} and thus on the variance of and covariance between the elements of a.

A different approach is the bootstrap method, which gives measures of uncertainties to sample estimates. The approach has been introduced by Bradley Elfron in 1979 [13]. Bootstrap is a computational method to find approximately a sampling distribution from the sample measured. The assumption made to formulate the approximation is that the measured data have to be independently and identically distributed (i.i.d.). Bootstrap substitutes the poorly known cumulative distribution function F_y by the empirical distribution function $\hat{F}_y$ of the measured data. Let $\hat{a}$ be an estimate for an unknown parameter. A bootstrap sample $y^*=\{y_1^*,y_2^*,\ldots y_n^*\}$ is produced by drawing n times at random with replacement from the measured data $y=\{y_1,y_2,\ldots y_n\}$. The generated sample has the same length as the original data. A bootstrap parameter estimate $\hat{a}^*$ is calculated from the bootstrap sample by fitting to y^*. For a large number B of bootstrap samples the distribution of $\hat{a}$ is approximated by the distribution of the bootstrap output $\hat{a}_1^*,\hat{a}_2^*,\ldots,\hat{a}_B^*$ [14–17].

The $(1-a)$ bootstrap percentile confidence interval (CI) for the corresponding parameter is given as:

$$\left[\hat{a}^{*\uparrow}\left((B+1)\frac{a}{2}\right),\ \hat{a}^{*\uparrow}\left((B+1)\left(1-\frac{a}{2}\right)\right)\right] \quad (3)$$

where $\hat{a}^{*\uparrow}$ are the bootstrap estimates in ascending order.

Considering the relative residuals, i.e. $(y_i\text{-}S_{Do})/y_i$, with $a=(S_o, S_1, S_2, S_3, \psi_1, \psi_2, \Delta)$, the assumption of i.i.d. data cannot be made. Clear residual structures can be seen in Fig. 1 taken from a typical polarimetry measurement.

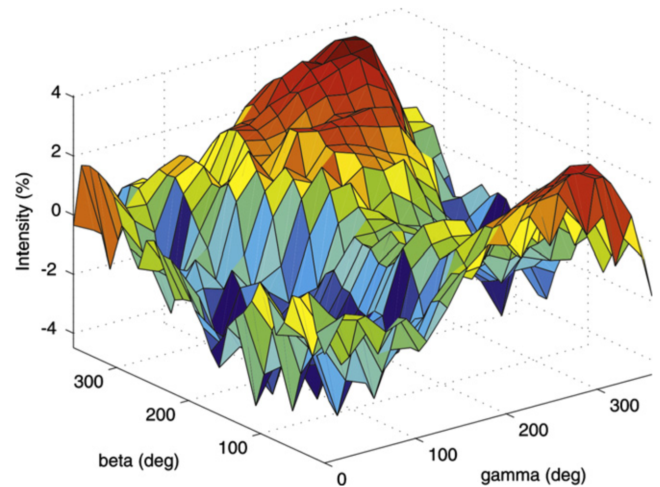

Fig. 1. Relative residuals of a typical polarization measurement.

One way to extend the basic bootstrap principle to dependent data is the block bootstrap [18,19]. Rather than re-sampling single data points the block bootstrap re-samples observations that are put together in blocks. As a result, the dependence structure of the original observation is preserved within each block. This weakens the assumption of i.i.d. data by assuming that only data points that are "far apart" have to be independent. The measurements close to each other remain in the dependency.

The bootstrap method is a mathematical approach to estimate statistical errors. Having systematic errors may lead to false results.

The validity of the block bootstrap in our case is tested with the following procedure (see Table 1):

1. Calculate signal values according to the polarimetry equation for given Stokes parameters, ψ_1, ψ_2 and phase retardance Δ.
2. Add the residuals from a measured data set to the values obtained in step 1.
3. Calculate estimates $\hat{a}$.
4. Create block bootstrap samples by putting eight measurement points, taken at the same β, in one block.

Author's personal copy

Table 1
Theoretical parameter values *a*, that have been chosen close to the estimated parameters from two polarization measurements â are the estimated values from the least χ^2-fit with corresponding 95% CI.

Test 1	a	â	95% CI	Test 2	a	â	95% CI
S_0	2080.0	2079.9	(2072.1, 2087.8)	S_0	2080.0	2080.0	(2072.5, 2088.0)
S_1	−0.050	−0.051	(−0.067, −0.046)	S_1	−0.050	−0.049	(−0.056, −0.043)
S_2	−0.090	−0.090	(−0.115, −0.085)	S_2	−0.050	−0.053	(−0.056, −0.043)
S_3	−0.9947	−0.9947	(−1.0000, −0.9911)	S_3	−0.9975	−0.9974	(−1.000, −0.9969)
$\psi 1$	0.750	0.750	(0.740, 0.750)	$\psi 1$	0.540	0.546	(0.527, 0.565)
$\psi 2$	0.300	0.299	(0.262, 0.432)	$\psi 2$	0.360	0.347	(0.296, 0.386)
Δ (rad)	−0.004	−0.004	(−0.018, 0.009)	Δ (rad)	−0.110	−0.107	(−0.118, −0.0964)

5. Fit the model function to the block bootstrap sample, thus determine block bootstrap estimates $\hat{a}^*$.
6. Repeat steps 4 and 5 B=5000 times to obtain the distribution of $\hat{a}^*$.
7. Calculate the 95% confidence interval.

All parameters are within the 95% CI, as listed in Table 1, i.e. the block bootstrap method gives reliable results in our case.

4. Results and discussion

4.1. Reflectivity measurements of the analyzer ML

The reflection analyzer is characterized by performing reflectivity measurements as a function of the incidence angle θ_A (Bragg curves) for different wavelengths of the incident light. The goal of the measurements is to independently characterize the analyzer ML. A good analyzer should have a large reflectance R_s and a large suppression ratio R_s/R_p. R_p is minimized at the Brewster angle and R_s is maximized at the Bragg angle, thus an ideal analyzer is one where the Bragg angle is equal to the Brewster angle.

Fig. 2 shows Bragg curves as function of θ_A for different wavelengths varying from 12.65 nm to 13.78 nm in p- and s-geometry. Fig. 3 illustrates the same in the range of 13.78 nm–14.59 nm. The thick curves outline a single Bragg curve at one wavelength. The large dots denote the measured maximal value, i.e. the peak reflectivity for each Bragg scan. Note that the angular position of the Bragg maximum and its width in s- and p-geometry are not identical.

Fig. 4(a) sums up the peak reflectivity of all measured Bragg curves shown in Figs. 2 and 3. According to Bragg's equation the peak position moves towards lower grazing angles for lower wavelengths and vice versa. S-reflectivity is nearly constant, while p-reflectivity goes through the Brewster minimum at 13.78 nm and $\theta_A = 48.4°$ ($R_p \approx 10^{-3}$). Fig. 4(b) shows the suppression ratio, which is at maximum at the Brewster angle ($R_s/R_p \approx 900$).

The large suppression ratio up to 900, as well as the high reflectivity up to 63%, justify the use of this MoSi ML as a polarization analyzer in the experimental setup in the investigated wavelength range.

Note that while crossing the Brewster angle the Kiessig fringes change character. At the Brewster angle the p-reflectivity is at a minimum. Going to either side of 13.78 nm, the p-reflectivity peak appears out of the +1 or −1 Kiessig fringe as shown in Fig. 5. This behavior is supported by theory as could be shown with the simulation program REFLEC [20].

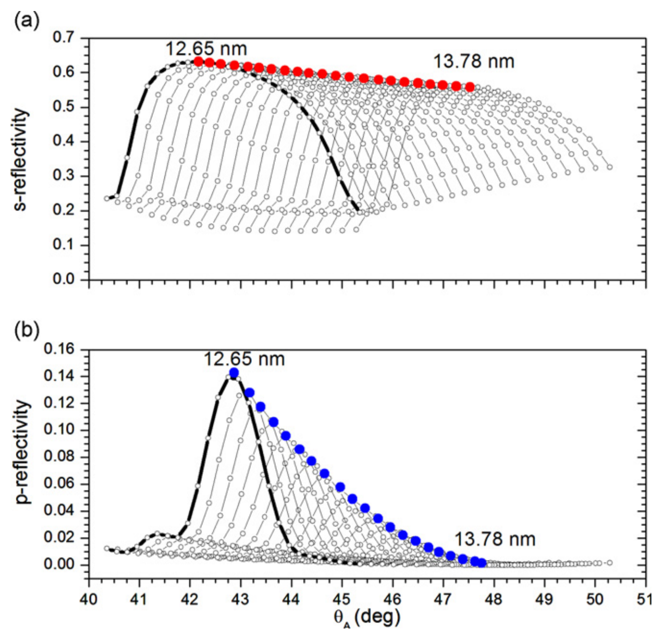

Fig. 2. Bragg curves of the analyzer ML for s-polarized (a) and p-polarized (b) light for a wavelength range of 12.65 nm–13.78 nm.

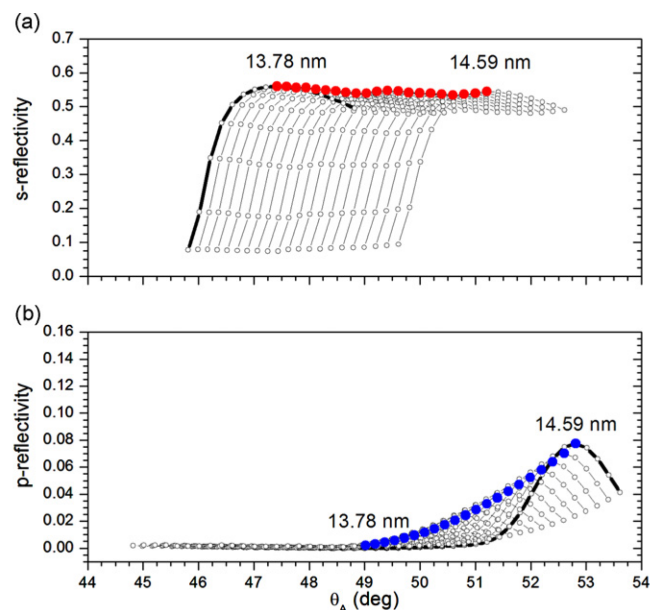

Fig. 3. Bragg curves of the analyzer ML for s-polarized (a) and p-polarized (b) light for a wavelength range of 13.78 nm–14.59 nm.

Author's personal copy

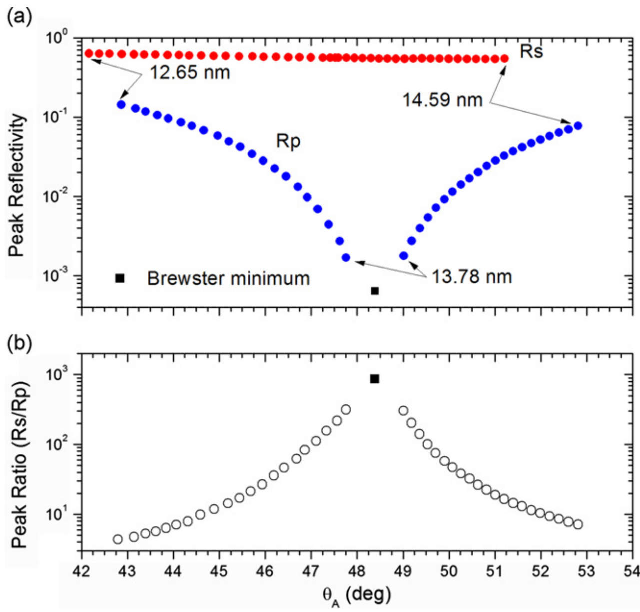

Fig. 4. (a) Sums up the peak reflectivity for s- and p-polarized light at different energies. The black square denotes the measured Brewster minimum of R_p taken from the measurements at 13.78 nm. (b) Shows the peak ratio R_s/R_p.

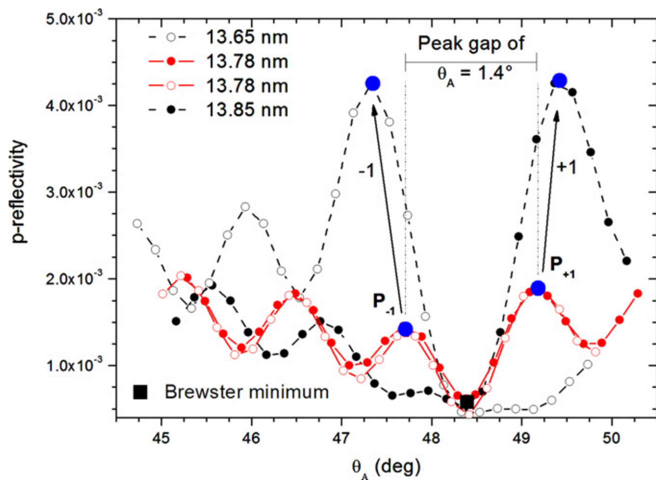

Fig. 5. Bragg curves for different energies in p-geometry. The large dots denote the peak reflectivity of each Bragg curve. The two solid curves show two different measurements at the same wavelength of 13.78 nm. With an increase or decrease of the wavelength two neighboring peaks P_{-1} and P_{+1} start to gain intensity following the -1 or $+1$ arrow accordingly.

4.2. Reflectivity measurements of the retarder ML

The reflectivity of the retarder ML measured as function of the wavelength for three different angles near normal incidence is shown in Fig. 6. Maximum R_s reflectivity of 67% was measured at 13.27 nm, maximum R_p reflectivity is 58% at 13.22 nm for $\theta_A=70°$. The difference between R_s and R_p decreases going towards normal incidence, as expected from Fresnel equations. Minor differences between model (calculation as provided by the supplier of the multilayer) and measurement can be seen regarding peak position. In the region of the Kiessig fringes the differences are more significant.

The measured reflectivity of the retarder ML at $\theta_A=70°$ will further be used in the polarimetry measurement (see Section 4.3) for the determination of the phase retardance Δ. Knowing the ratio R_p/R_s allows the free parameter ψ_1 ($\tan\psi_1=\sqrt{R_p/R_s}$) to be fixed within the polarimetry Eq. (1). Using the measured data for this ratio reduces the fitting equation by one degree of freedom and thus makes the fit more stable. Additionally the fitting parameter Δ is highly correlated with ψ_1 and fixing ψ_1 eliminates the uncertainty due to this correlation.

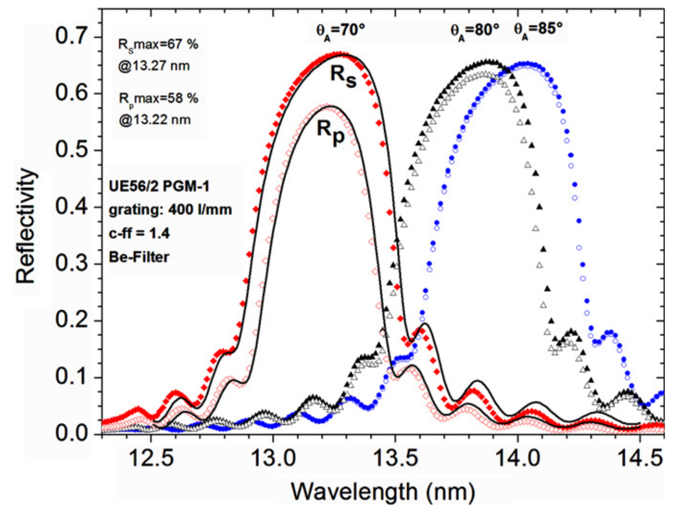

Fig. 6. Reflectivity measurements for s- and p-polarized light. The incident angle at 20°, 10° and 5° off normal, was kept fixed while varying the wavelength. The two solid lines are model calculations performed for 20° off normal incidence.

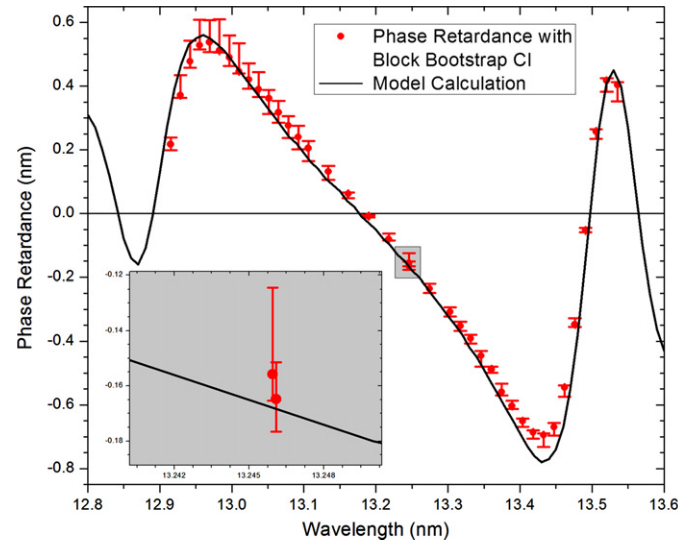

Fig. 7. Phase retardance for the Mo/Si ML with confidence intervals calculated via the block bootstrap method obtained with circularly polarized light. The gray enlarged area shows two measurements taken at the same wavelength.

4.3. Phase retardance of the retarder ML

Polarization measurements were performed to determine the phase retardance according to the polarimetry Eq. (1). The grazing incidence of the retarder was set to $\theta_A=70°$, while the analyzer was set to the angle corresponding to the maximum Bragg reflectivity for the particular wavelength being measured. Under these conditions the azimuthal angles β and γ were varied over full 360° available. The polarization of the radiation was set to right-hand circularly polarized light, i.e. the Stokes parameter S_3 is -1. Another data set was taken with linearly polarized light. The β stage held the retarder ML in reflection geometry and produced a phase retardation between the two orthogonal electric field components of the incoming light. The γ stage held the

Author's personal copy

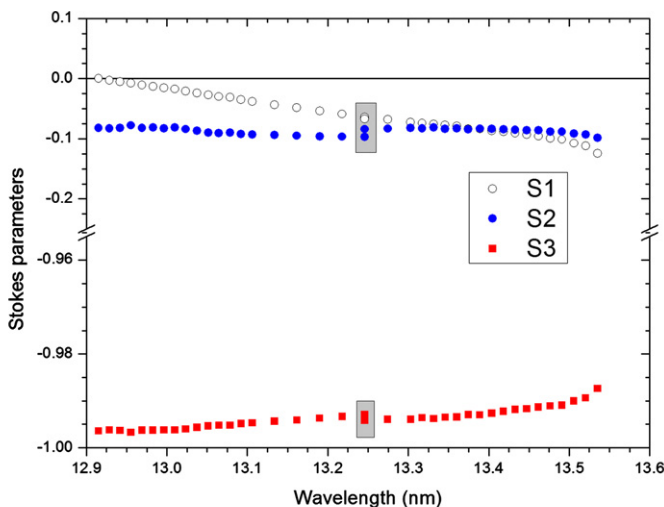

Fig. 8. Stokes parameters determined from the polarimetry measurement of the UE56/2 PGM-1 beamline. The gray square indicates two measurements taken at the same wavelength. Reduction is due to tuning range limitation of the UE56 in circular mode.

analyzer, which was operated near the Brewster angle. The previously independently measured ratio of R_p/R_s (Fig. 6) was used in fitting the polarimetry Eq. (1) to the measured data.

Fig. 7 shows the phase retardance Δ and the model calculation as function of wavelength for the retarder ML. This data set was obtained using circularly polarized light. The error bars in Fig. 7 were estimated via the block bootstrap method. The blocks were created by putting eight neighboring measurements, taken at the same β, within one block. The calculation was performed once with a free parameter ψ_1 and once with a fixed one. In each case the largest value of the calculated 95% CI was taken as a corresponding error bar. That way the influence of the uncertainties of the ratio R_p/R_s were taken into account in the CI of the phase retardance.

The phase retardance is in good agreement with the model calculation except for the region around 13.44 nm. Maximum phase retardance stays below 0.7 nm. The phase retardance at maximum R_s reflectivity at 13.27 nm is $\Delta = -0.23$ nm. Δ changes sign at 13.18 nm.

The block bootstrap CI gives an accuracy of the phase retardance better than 0.1 nm. Data points taken twice at the same wavelength agree in their corresponding CI as can be seen in the gray enlarged area within Fig. 7.

The measurements taken with linearly polarized light show physically non-plausible results. Within the polarimetry Eq. (1) the only terms depending on Δ are two cosine functions. Thus χ^2 depends only weakly on Δ, when Δ is small. The sign of the phase retardance is undetermined.

4.4. Beamline polarization

As a by-product of the ML characterization the characterization of the beamline is accomplished with respect to the complete polarization state. Fig. 8 shows the measured Stokes parameters of the beamline UE56/2 PGM-1. The fraction of circularly polarized light S_3 decreases going towards longer wavelengths, which is consistent with the undulator settings. The undulator may be tuned to give nominally fully circularly polarized radiation up to approx. 13 nm. Beyond this tuning range the motion of the magnets is limited and the output becomes increasingly elliptical with an increasing proportion of S_1 being produced at the expense of the circular mode. Within the tuning range the average value of S_3 is -0.9963 with a standard deviation smaller than 10^{-3}.

5. Summary

We have characterized the reflectivity of Mo/Si MLs and determined the relative phase retardance in the EUV range with polarized synchrotron radiation. Block bootstrap method was used to determine an error of the phase retardance values to ensure a reliable verification of the ML-model. The phase retardance was always less than 0.7 nm across the Bragg peak and the Kiessig fringes with an accuracy of 0.1 nm. Minor differences can be seen between the model calculation and the measurement for the reflectivity as well as the phase retardance.

Our ellipsometry technique is an additional sensitive probe to characterize ML optical elements and it enables complete at-wavelength characterization. Measurement of complex reflection coefficient allows a more refined test of the ML model, including interdiffusion layers and interface structure. Information on the phase retardance improves the control of the wavefront and thus of the imaging resolution in EUV systems. The use of circularly polarized light is essential for the phase retardance determination.

In addition the complete polarization state of the beamline UE56/2 PGM-1 in the EUV range is determined from the polarimetry measurement with a precision of 0.1%.

Acknowledgment

This project was financially supported by the Zeiss SMT GmbH.

References

[1] G. Tallents, E. Wagenaars, G. Pert, Nature Photonics 4 (2010) 809.
[2] C. Laubis, et al., SPIE-Proceedings 7636 (2010) 76362R.
[3] F. Schäfers, et al., Applied Optics 38 (1999) 4074.
[4] A. Gaupp, F. Schäfers, M. MacDonald, S. Uschakow, N.N. Salashchenko, P.K. Gaykovich, Carbon K-edge Polarimetry with Cr/Sc Transmission Multilayers, Proceedings SRI-12, Journal of Physics IOP Conference Series, in press.
[5] M. MacDonald, F. Schäfers, A. Gaupp, Optics Express 17 (25) (2009) 23290.
[6] S. Uschakow, Optical Characterization of Novel Mosi Multilayer Systems for the Next Generation of Lithography in the EUV Range With Polarized Synchrotron Radiation, Masterthesis, Freie Universität Berlin, Physics Departement (2012).
[7] S. Uschakow, A. Gaupp, M. MacDonald, F. Schäfers, Part was Published at the 11th SRI conference: EUV Ellipsometry on Mo/Si multilayers, Proceedings SRI-12, Journal of Physics IOP Conference Series, in press.
[8] S. Valencia, A. Kleibert, A. Gaupp, J. Rusz, D. Legut, J. Bansmann, W. Gudat, P.M. Oppeneer, Physical Review Letters 104 (2010) 187401.
[9] A. Gaupp, M. Mast, Review of Scientific Instruments 60 (1989) 2213.
[10] A. Gaupp, W. Peatman, SPIE 733 (1986) 272.
[11] M.R. Weiss, et al., Nuclear Instruments and Methods in Physics Research A 467 (2001) 449.
[12] S. Sasaki, K. Miyata, T. Takada, Japanese Journal of Applied Physics 31 (1992) L1794.
[13] B. Elfron, Annals of Statistics 7 (1979) 1.
[14] A.M. Zoubir, D. Robert Iskander, IEEE Signal Processing Magazine 24 (4) (2007) 10–19.
[15] B. Elfron, R. Tibshirani, An Introduction to the Bootstrap, first ed., Chapman & Hall/CRC, London, 1994.
[16] D.N. Politis, IEEE Signal Processing Magazine 15 (1998) 39.
[17] B. Elfon, Statistical Science 18 (2) (2003) 135.
[18] H. Kuensch, Annals of Statistics 17 (3) (1989) 1217.
[19] N. Lahiri, Resampling Methods for Dependent Data, first ed., Springer, New York, 2010.
[20] F. Schäfers, M. Krumrey, Technischer Bericht, BESSY TB 201 (1996) 1.